Nuclear Instruments and Methods in Physics Research A 663 (2012) 22–25

Contents lists available at SciVerse ScienceDirect

Nuclear Instruments and Methods in Physics Research A

journal homepage: www.elsevier.com/locate/nima

Study of spatial resolution properties of a glass RPC

Qite Li, Yanlin Ye *, Chao Wen, Wei Ji, Yushou Song, Rongrong Ma, Chen Zhou, Yucheng Ge, Hongtao Liu

School of Physics and State Key Laboratory of Nuclear Physics and Technology, Peking University, Beijing 100871, China

ARTICLE INFO

Article history:
Received 22 February 2011
Received in revised form
22 July 2011
Accepted 7 October 2011
Available online 18 October 2011

Keywords:
Resistive plate chamber
Signal charge profile
Spatial resolution
Delay-line

ABSTRACT

A prototyping glass RPC with excellent signal-to-noise ratio was constructed and tested. Detection efficiencies for cosmic rays of about 95% were obtained for both avalanche and streamer modes of operation. A simple method to measure the signal charge profile is developed, which is consistent with other methods such as direct optical observation. A narrow profile for avalanche signal mode is obtained, which may lead to an intrinsic spatial resolution less than 1.0 mm FWHM. If a delay-line or charge division technique is used to determine the centroid of the signal charge distribution, it is important to reduce the electronics noise and the fluctuations of the delay-line (or resistor) units in order to reach the ultimate intrinsic position resolution.

1. Introduction

The Resistive Plate Chamber (RPC) has been known as a large-size gas detector with several important advantages: simple and robust structure, long time stability, good time resolution and low cost [1–3]. It can be operated in streamer mode or avalanche mode, depending on the requirement of specific applications [4]. In the streamer mode the signal-to-noise ratio is very high, but the detection dead-time is relatively long and therefore the sustainable counting rate is quite limited. In contrast in the avalanche mode high counting rate can be achieved, but the signal is relatively small and the front-end electronics is required to pre-amplify the primary signal. Based on intensive studies large size RPCs have been widely used in high energy physics experiments such as CMS at LHC [5,6], cosmic-ray physics experiments such as ARGO-YBJ [7] and neutrino physics experiments such as OPERA [8]. In the last years small size timing RPCs have also been developed [9,10] and applied to some high energy and nuclear physics experiments such as ALICE [8], HADES [11] and FOPI [12]. These applications require very high counting rates or excellent timing resolutions, but only moderate position resolutions (a few centimeters). As a result position resolution has been a much less studied property of large size RPCs [3,13].

In the recent years muon tomography has attracted much attention due to its possible application to detect high Z materials [14–16]. Precise measurements of the incident and outgoing angles of the cosmic muons are mandatory in this application, whereas counting rate capability is not a problem since the intensity of cosmic rays is very low (about 1 muon/cm^2/min). Large size RPC should be an ideal candidate for the detector system if its spatial resolution could attain a level of less than 1 mm, meanwhile keeping its build-in advantages as indicated above [2]. Spatial resolution is closely related to the size of the signal charge distribution inside the detector gas volume. Generally the avalanche signal has smaller size for its change distribution and therefore should be more suitable for cosmic ray tracking, compared to the streamer signal. Moreover the signal charge distribution might spread over the semi-conductive electrode (normally made of a resistive plate coated by a thin layer of graphite), resulting in worse spatial resolution. Therefore it would be necessary to study the signal charge distribution quantitatively at the readout stage in order to obtain the optimum spatial resolution.

In the history of RPC development, operation modes were carefully investigated for various gas mixtures, electrode resistivity, applied high voltage (HV), and so on [4,17,18]. Signal charge distribution was studied for streamer mode [18–20]. A precise position measurement method was tested by using the process of signal spreading on the graphite layer [20]. But the applicability of this method is limited by the rapid decrease of the signal amplitude when propagating on the two-dimensional surface towards the edges of the electrode. One test for avalanche signal profile was reported [21] but the applied gas mixture was not appropriate for a good operation in avalanche mode [17].

We report here the performance of a glass RPC, emphasizing the measurement of the signal charge distributions for both streamer and avalanche modes. These distributions would serve to estimate the ultimate spatial resolution of the large size RPC.

2. Description of the glass RPC and the detection setup

Resistive plates are basic components to build a RPC. The bulk resistivity of the plate could be varied to meet the needs of

* Corresponding author. Tel.: +86 10 62761193; fax: +86 10 62751875.
E-mail address: yeyl@pku.edu.cn (Y. Ye).

0168-9002/$ - see front matter © 2011 Elsevier B.V. All rights reserved.
doi:10.1016/j.nima.2011.10.006

different applications. For instance lower resistivity is in favor of high counting rate but would lead to worse spatial resolution [5,22]. It was demonstrated that commercial float glass, due to its stability, long range homogeneity, excellent surface smoothness etc, could be a good alternative to bakelite electrode [1,23].

As shown in Fig. 1, a glass RPC was built in our laboratory by using 2.6 mm thick float-glass plates, each with an area of 30*30 cm^2. The gas gap between the gas plates was accurately fixed by spacers of 2 mm height. The electrodes were made of thin graphite layers coated on the glass plates, with surface resistivity of about 10^7 Ω/sq. The effective area of the electrode was 20*20 cm^2. 2.54 mm wide readout strips were integrated on a printed-circuit board placed beneath the glass plate. Both ends of each strip were connected to delay-lines with 4 ns delay between every adjacent two strips. Signals from both ends of a delay-line were fed into 300 MHz fast preamplifiers. According to the design of the printed board, it was also possible to read out signals strip by strip, which is useful to determine the charge profile of a signal in the gas gap.

The whole RPC was placed inside a gas-tight Aluminum box. Mixed gases of 90% F_{134a}+9% iso-C_4H_{10}+1% SF_6 were supplied to the box, with a flow rate of about 50 cm^3/min. A small portion of SF_6 is used to retard the appearance of streamer signals [17].

The tests were conducted by using cosmic rays. The schematic diagram of RPC testing setup is shown in Fig. 2. Two finger type plastic scintillation counters, each having a size of $14.5 \times 3 \times 0.5$ cm^3, were placed on top of the test RPC in order to coincidentally trigger

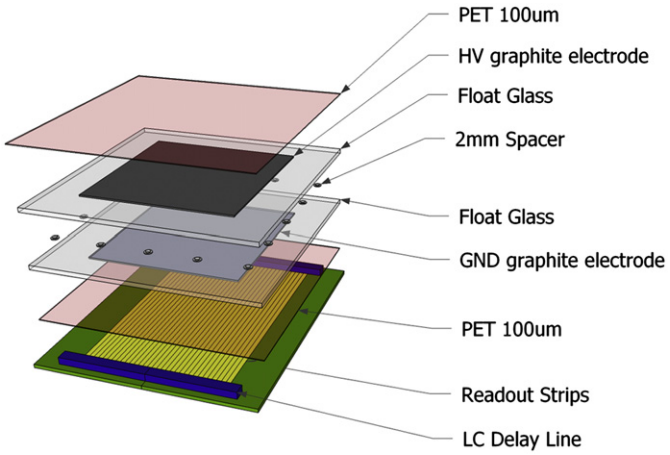

Fig. 1. Layout of the glass RPC.

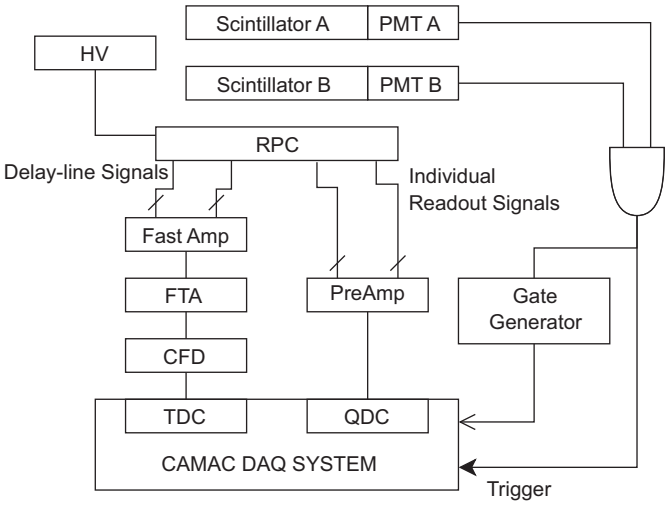

Fig. 2. Schematic diagram of RPC testing system.

cosmic rays. Timing signals taken from both ends of the chain of delay-line units, were fed into 300 MHz fast preamplifiers (Ortec 820 with a gain of 200 and a equivalent input noise of ≤ 20 μV rms), and then sent to Fast Timing Filter Amplifiers (Ortec 863, with a noise level < 50 μV and a differentiation time constant set at 200 ns). Constant Fraction Discriminators (CFD) were used to reduce time walk effect. In order to acquire the induced charge profile, signals can also be read from individual readout strips and fed into voltage sensitive preamplifiers (PreAmp, with a bandwidth of 10–320 MHz, a gain of 800 and a noise level less than 40 μV). Charges contained in these signals were digitized by a 12 Bit QDC with a time window of 150 ns. Data were recorded by a CAMAC system.

3. Test results

3.1. Original signals of the RPC

This glass RPC can sustain a high voltage (HV) up to 13 kV while keeping a dark current much lower than that for RPCs made of normal Bakelite [5]. Fig. 3(A) shows a pure avalanche signal taken directly from a readout strip and viewed by a digital oscilloscope, while Fig. 3(B) presents an avalanche signal followed by a much larger streamer signal [4]. It is worthy to note the remarkably high signal-to-noise ratio even for the small avalanche signal, compared with that of the previous RPC made of resistive bakelites [22]. This is a direct and important indication of the very good quality of this glass RPC, which in turn determines its excellent basic performances.

3.2. Detection efficiency

Because of the large difference between the amount of charges contained in an avalanche signal (a few pC) and in a streamer signal (50 pC or more) [4,17], we set 2 threshold values to determine the efficiencies, with the higher one allowing only the streamer signal to pass through [17]. At low counting rate the detection efficiency of the RPC may be defined as:

$$\varepsilon(HV) = \frac{N_{RPC}(HV)}{N_{Sci}(HV)}$$

where $N_{Sci}(HV)$ is the number of cosmic ray signals taken coincidentally by the scintillator pair, and $N_{RPC}(HV)$ the number further in coincidence with the RPC. The efficiencies as a function of the applied high voltages (HV) are plotted in Fig. 4. In the figure it can be seen that both avalanche and streamer detection efficiencies can reach 95%. There is about 1000 V shift between the avalanche efficiency curve and the streamer efficiency curve. It is demonstrated that the current glass RPC may operate in a pure avalanche mode at around 9.5 kV, or in a pure streamer mode at voltages higher than 11 kV.

3.3. Charge profiles

The spatial resolution of a RPC is closely related to the internal signal charge distribution. One internal signal may induce charges on several strips. Therefore for each triggered cosmic event we read out charges strip by strip and then the charge distribution can be extracted. In order to build good statistics, we tried to match the peak positions of the distributions for all detected events. This means that for each event, firstly, we determine the center of the distribution by using the charge weighted average method. This center position is then shifted to 0 point along the X coordinate. Secondly for each fired read-out strip the X position is determined according to its distance to the center, while the vertical coordinate is defined as the ratio of the readout charge

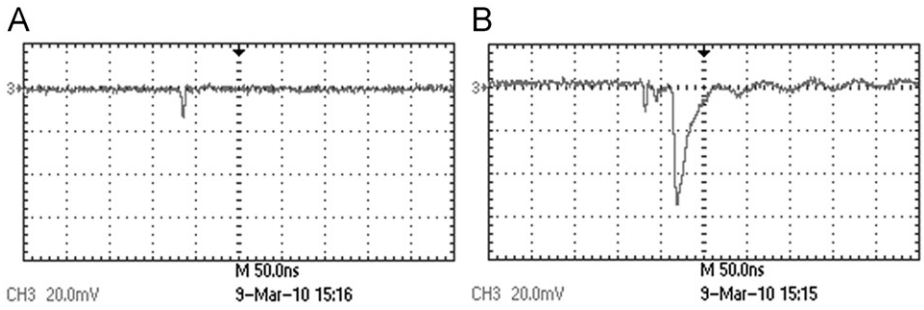

Fig. 3. (A) Direct view of a pure avalanche signal and (B) a avalanche signal followed by a streamer signal, as viewed by the digital oscilloscope channel 3 (CH3).

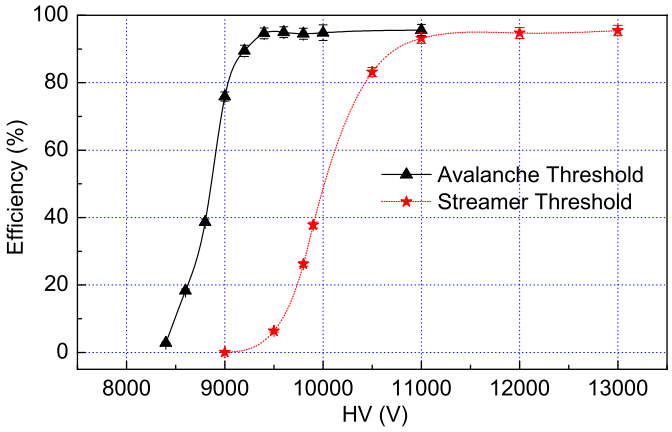

Fig. 4. Efficiency curves for the glass RPC.

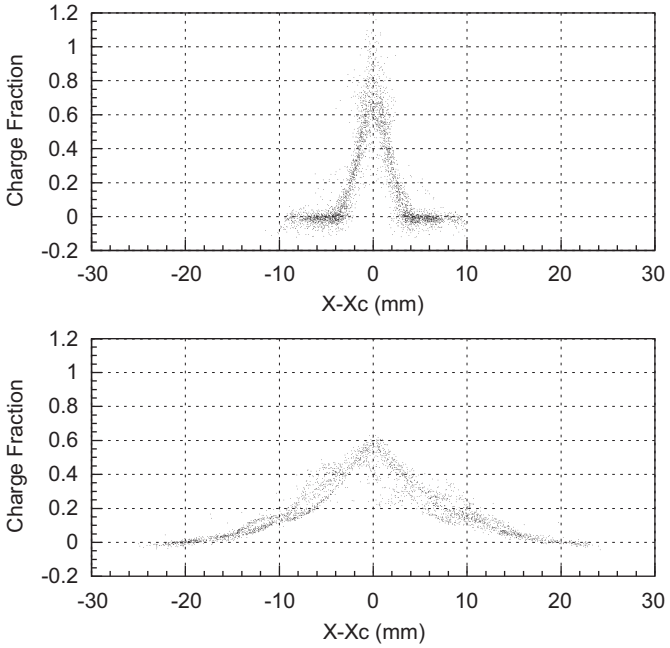

Fig. 5. Induced charge profiles of avalanche signals (upper figure) and streamer signals (lower figure). The FWHM of the profile is about 4 mm for the former and about 12 mm for the latter.

taken from that strip relative to the total charge of the signal. The results are presented in Fig. 5.

In the lower picture of Fig. 5 we see a charge profile for streamer mode as wide as 12 mm (FWHM) or so, which should include contributions from the size of the original discharge in the gas gap and from the effect of charge spreading on the graphite layer. The width of the profile measured here is similar to the previously reported results [19]. It is interesting to see a much narrower charge profile for avalanche signals (upper picture of Fig. 5). The width (FWHM) is now about 4 mm, only one third of that for streamer signal. Similar size (2–4 mm in diameter) for a single avalanche (or discharge) was also observed with a direct optical method [18] or a fitting method [21], when appropriate gas mixture was chosen. Therefore we may estimate that for the current RPC running in avalanche mode, the measured signal charge profile is basically determined by the avalanche process in the gas gap, instead of being affected by signal spreading on the graphite layer. As a matter of fact the charge propagating on a thin graphite layer is much slower (a few cm per micro-second) than that on a readout strip [20]. It is reasonable that the charge profile based on the strip readout has little correlation with the property of the graphite layer.

3.4. Estimation for spatial resolution

For applications such as cosmic ray tomography, it is very important for the detection system to have excellent spatial resolution [15]. Since counting rate is low for cosmic rays, the delay-line or charge-division method could be applied, which allows to largely reduce the number of readout channels and related electronics, meanwhile keeping good spatial resolution through the determination of the centroid of the signal charge distribution [13]. The statistical uncertainty of the centroid position is proportional to the width of the signal charge profile. This uncertainty might be treated as the ultimate intrinsic position resolution of the RPC, or the limit for determining the position resolution through the delay-line or charge-division method [24]. For avalanche mode operation of a RPC, this statistical uncertainty may be as low as 0.5 mm, as analyzed in Ref. [21].

But other factors might prevent to achieve this ultimate limit. One particular problem for the current readout system is the non-uniformity of the delay-line or charge-division (resistor) units, in addition to the general electronics fluctuations, which should be superposed to the intrinsic position resolution. To evaluate the performance of the actual delay line circuit, we used the same kind of delay line at both sides of the strips. The trigger scintillators were placed perpendicular to the strips and across the mid-points of them. In this way, we obtain two positions for each triggered cosmic event, namely X1 and X2, from 2 sides of the readout strips. If the readout circuit is 100% uniform and the electronics noise is negligible, X1–X2 should be exactly zero. In reality we obtain approximately a Gaussian peak distribution with a FWHM of 1.34 mm, as shown in Fig. 6. Since we only need delay line at one side of the strips in a real measurement, the introduced uncertainty should be $1.34\,\mathrm{mm}/\sqrt{2} = 0.95\,\mathrm{mm}$. This systematic error due to the non-uniformity of the delay line units, together with readout electronics fluctuation, is even larger than

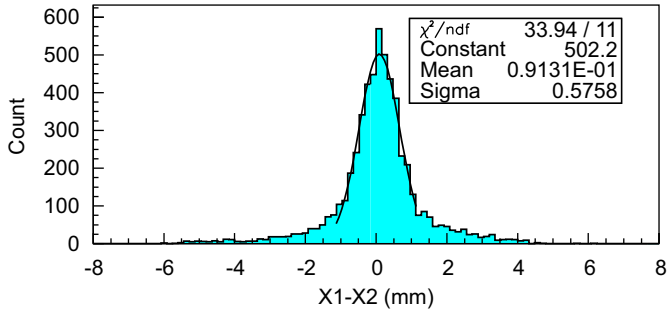

Fig. 6. Distribution of X1-X2 as explained in the text, with a Gaussian function fit (Sigma=0.57 mm and FWHM=1.34 mm).

the intrinsic position resolution. It is clear that the performance of the readout system must be improved before going further to achieve a position resolution of less than 1 mm.

4. Summary

A prototyping glass RPC with excellent signal-to-noise ratio was successfully designed, constructed and tested. Detection efficiencies of about 95% were obtained for both avalanche and streamer modes of operation. A simple method to measure the signal charge profile is developed, which is consistent with other methods such as direct optical observation. It is shown that the width of the profile for avalanche mode is only one third of that for streamer mode, indicating the inherent advantage of using the avalanche mode to make precise position measurement. Based on the profile analysis, an intrinsic spatial resolution less than 1.0 mm in FWHM is expected. Due to the low counting rate for cosmic ray tomography, it would be good to apply delay-line or charge division technique for the readout system in order to reduce the number of electronics channels, but the fluctuations of the delay-line (or resistor) units and related electronics must be reduced in order to reach the ultimate intrinsic position resolution. It is encouraged to build a system with several layers of RPCs to directly measure the position resolution at different conditions of gas mixture, surface resistivity of the graphite layer, high voltage and readout technique.

Acknowledgments

This work is supported by the National Natural Science Foundation of China (nos. 10821140159, 10827505, 11035001, 10775003 and J0730316), and the National Basic Research Program of China (no. 2007CB815002).

References

[1] P. Fonte, IEEE Transactions on Nuclear Science 49 (2002) 881.
[2] R. Santonico, Nuclear Physics B 158 (2006) 5.
[3] R. Santonico, Nuclear Instruments and Methods in Physics Research Section A: Accelerators, Spectrometers, Detectors and Associated Equipment (2010). doi:10.1016/j.nima.2010.08.080.
[4] R. Cardarelli, V. Makeev, R. Santonico, Nuclear Instruments and Methods in Physics Research Section A: Accelerators, Spectrometers, Detectors and Associated Equipment 382 (1996) 470.
[5] J. Ying, Y.L. Ye, Y. Ban, et al., Nuclear Instruments and Methods in Physics Research Section A: Accelerators, Spectrometers, Detectors and Associated Equipment 459 (2001) 513.
[6] Z. Aftab, et al., Nuclear Physics B 158 (2006) 103.
[7] G. Aielli, et al., Nuclear Instruments and Methods in Physics Research Section A: Accelerators, Spectrometers, Detectors and Associated Equipment (2010), 10.1016/j.nima.2010.09.066.
[8] A. Bertotin, et al., Nuclear Instruments and Methods in Physics Research Section A: Accelerators, Spectrometers, Detectors and Associated Equipment 602 (2009) 631.
[9] C. Finck, et al., Nuclear Instruments and Methods in Physics Research Section A: Accelerators, Spectrometers, Detectors and Associated Equipment 508 (2003) 63.
[10] A. Blanco, et al., Nuclear Instruments and Methods in Physics Research Section A: Accelerators, Spectrometers, Detectors and Associated Equipment 508 (2003) 70.
[11] K. Aamodt, the ALICE collaboration, et al., Journal of Instrumentation 3 (2008) S08005.
[12] A. Schuttaut, et al., Nuclear Instruments and Methods in Physics Research Section A: Accelerators, Spectrometers, Detectors and Associated Equipment 602 (2009) 679.
[13] R. Santonico, Nuclear Instruments and Methods in Physics Research Section A: Accelerators, Spectrometers, Detectors and Associated Equipment 533 (2004) 1–6.
[14] K.N. Borozdin, G.E. Hogan, C. Morris, et al., Nature 422 (2003) 277.
[15] L.J. Schultz, et al., Nuclear Instruments and Methods in Physics Research Section A: Accelerators, Spectrometers, Detectors and Associated Equipment 519 (2004) 687–694.
[16] C.L. Morris, C.C. Alexander, J.D. Bacon, et al., Science and Global Security 16 (2008) 37.
[17] P. Camarri, et al., Nuclear Instruments and Methods in Physics Research Section A: Accelerators, Spectrometers, Detectors and Associated Equipment 414 (1998) 317–324.
[18] I. Kitayama, H. Sakai, Y. Teramoto, et al., Nuclear Instruments and Methods in Physics Research Section A: Accelerators, Spectrometers, Detectors and Associated Equipment 424 (1999) 474.
[19] R. Arnaldi, A. Baldit, B. Barret, et al., Nuclear Instruments and Methods in Physics Research Section A: Accelerators, Spectrometers, Detectors and Associated Equipment 490 (2002) 51.
[20] R. Cardarelli, G. Aielli, P. Camarri, et al., Nuclear Instruments and Methods in Physics Research Section A: Accelerators, Spectrometers, Detectors and Associated Equipment 572 (2007) 170.
[21] J. Ye, J.P. Cheng, Q. Yue, et al., Nuclear Instruments and Methods in Physics Research Section A: Accelerators, Spectrometers, Detectors and Associated Equipment 591 (2008) 411.
[22] J. Ying, Y.L. Ye, Y. Ban, et al., Journal of Physics G: Nuclear and Particle Physics 26 (2000) 1291.
[23] A. Calcaterra, et al., Nuclear Instruments and Methods in Physics Research Section A: Accelerators, Spectrometers, Detectors and Associated Equipment 533 (2004) 154.
[24] Y.L. Ye, Z.Y. Di, Z.H. Li, et al., Nuclear Instruments and Methods in Physics Research Section A: Accelerators, Spectrometers, Detectors and Associated Equipment 515 (2003) 718.